Spin-dependent electron scattering at graphene edges on Ni(111)

A. Garcia-Lekue,[1,2] T. Balashov,[3] M. Olle,[3] G. Ceballos,[3] A. Arnau,[1,4,5] P. Gambardella,[3,6,7] D. Sanchez-Portal,[1,4] and A. Mugarza[3]

[1]*Donostia International Physics Center (DIPC), Paseo Manuel de Lardizabal 4, E-20018 San Sebastián, Spain*
[2]*IKERBASQUE, Basque Foundation for Science, E-48011, Bilbao, Spain*
[3]*Catalan Institute of Nanoscience and Nanotecnology (ICN2), UAB Campus, E-08193 Bellaterra, Spain*
[4]*Centro de Física de Materiales CFM - MPC, Centro Mixto CSIC-UPV, Apdo. 1072, San Sebastián, Spain*
[5]*Dpto. de Física de Materiales UPV/EHU, Facultad de Quimica, Apdo. 1072, San Sebastián, Spain*
[6]*Instituciò Catalana de Recerca i Estudis Avancats (ICREA), E-08193 Barcelona, Spain*
[7]*Department of Materials, ETH Zurich, Schafmattstrasse 30, CH-8093 Zurich, Switzerland*

(Dated: December 14, 2013)

We investigate the scattering of surface electrons by the edges of graphene islands grown on Ni(111). By combining local tunneling spectroscopy and *ab initio* electronic structure calculations we find that the hybridization between graphene and Ni states results in strongly reflecting graphene edges. Quantum interference patterns formed around the islands reveal a spin-dependent scattering of the Shockley bands of Ni, which we attribute to their distinct coupling to bulk states. Moreover, we find a strong dependence of the scattering amplitude on the atomic structure of the edges, depending on the orbital character and energy of the surface states.

Understanding electron scattering at graphene edges and domain boundaries is fundamental to control transport and quantum confinement in graphene-based electronic devices [1–3]. Edges and boundary defects play an important role in electron transport across multidomain, mesoscopic graphene layers [4, 5], as well as in inducing energy gaps [6, 7] and magnetic order [8] in graphene nanostructures.

A particularly relevant issue for the performance of nanodevices is the scattering of electrons at the interface between graphene and metal contacts, which determines the charge and spin injection efficiency into graphene. Weakly interacting metal contacts simply dope the Dirac bands [9, 10]. In such a case, scattering depends only on the energy match between undistorted graphene and metal states. The interface with more reactive metals, however, is usually characterized by significant electronic reconstruction, which defines a complex scenario for scattering. The graphene/Ni interface represents an interesting case where the interaction with the ferromagnetic substrate opens hybridization gaps [11–14] and induces magnetic moments [15]. Consequently, graphene is predicted to behave as a perfect spin-filter in contact with a magnetic Ni electrode [13, 14], as suggested also by the high spin injection efficiency measured in $Ni_{80}Fe_{20}$/graphene/Si heterostructures [16]. Previous studies focused on electron injection perpendicular to the interface, whereas edge scattering in the most common current-in-plane geometry, remains unexplored.

In this Letter, we investigate electron scattering at the edges of graphene on a Ni(111) substrate. We grow graphene nanoislands with well-defined edge geometries in order to simultaneously probe the electronic structure of the vertical and lateral graphene interfaces and compare it with that of the pristine Ni surface. We find clear signatures of spin- and edge-dependent electron scattering revealed by local tunneling spectroscopy measurements combined with spin-polarized *ab initio* electronic structure calculations. This behavior is attributed to the strong distortion of the electronic structure at the interface, where the Ni surface states significantly shift in energy and space due to the confinement induced by the graphene layer, and to the different coupling to bulk states of majority and minority Ni states. We further demonstrate that edge scattering is strongly structure dependent, with asymmetries in the reflection amplitude of up to 30% for reconstructed and non-reconstructed zigzag edges. These results suggest the possibility of lateral spin-filtering for graphene layers, and demonstrate the importance of designing nanostructures with well-defined edges to control electron/spin transport and confinement in graphene.

The experiments were performed using a scanning tunneling microscope (STM) operated at 5 K in ultrahigh vacuum (UHV). The Ni(111) single crystal was cleaned in UHV by cycles of Ar^+ sputtering and annealing to 925 K. Graphene nanoislands were grown from the catalytic decomposition of propene (C_3H_6) on a clean Ni(111) single crystal. Islands with straight edges and either triangular or hexagonal shape were obtained by controlling the reaction temperature and annealing conditions, following the method presented in Ref. 17. Spectroscopic measurements were performed by STM using the lock-in technique, with a bias voltage modulation of frequency 3 kHz and amplitude 1 mV_{rms} for the dI/dV spectra, and of 15 mV_{rms} for the dI/dV maps. The *ab initio* calculations of the electronic structure were carried out using density functional theory (DFT), as implemented

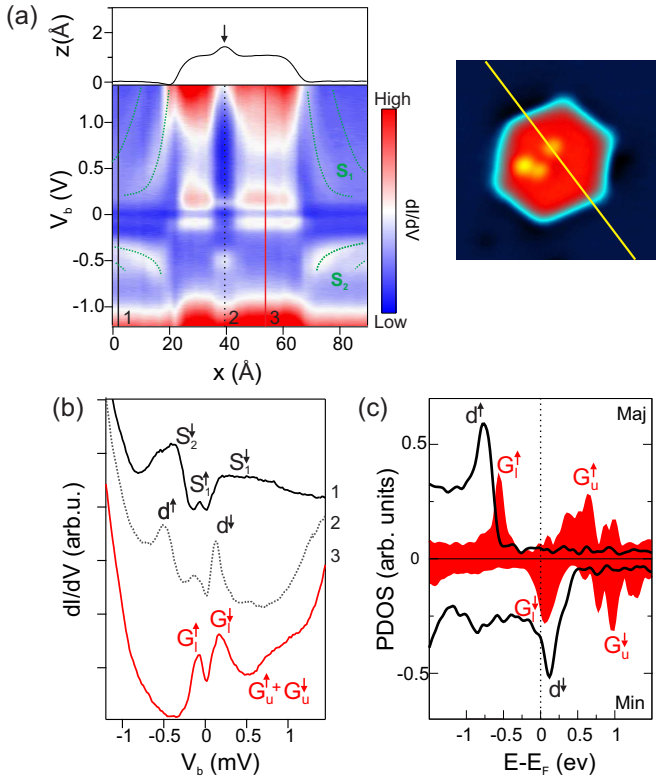

FIG. 1. (Color online) (a) Topographic profile and constant height dI/dV spectra taken along the yellow line that crosses the hexagonal island in the STM image shown on the right. The standing waves arising from scattering of the S_1 and S_2 surface states are indicated by green lines. Setpoint values: $I = 4$ nA, $V_b = -3.0$ V. (b) dI/dV spectra of the Ni surface (black), graphene island (red), and of a Ni impurity in the island (dotted grey). (c) Calculated density of states of majority and minority states, projected onto C (red areas) and Ni (black line) atoms. Graphene bands are labeled as $G^{\uparrow/\downarrow}_{u/l}$ for spin up/down ($\uparrow$ / $\downarrow$) and upper and lower band (u/l). For visualization purposes, the PDOS of Ni has been divided by 50.

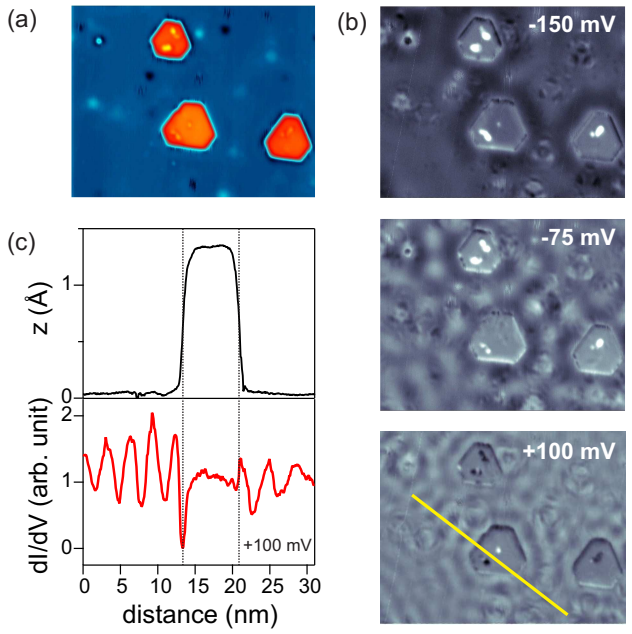

FIG. 2. (Color online) (a) Topographic ($V_b = 0.1$ V) and (b) constant current dI/dV maps simultaneously acquired at different energies, showing the interference patterns of the S_1 surface state scattered from graphene islands. Setpoint current: $I = 0.3$ nA. Image size: 30×37 nm^2. (c) Topographic and dI/dV profiles along the yellow line in (b), illustrating the absence of interference patterns inside the island.

in the SIESTA code [18]. We use a supercell description of the system, consisting of a slab containing 13 layers of Ni(111), covered by a single graphene layer on each side. For pristine Ni(111), we employ a 19-layer slab in order to avoid interactions between surface states on the two opposite sides. Further details on the calculations are given in the Supplementary Material [19].

We investigate first the local electronic structure of the graphene islands and surrounding Ni surface, focusing on how the electronic states of both graphene and Ni are mutually perturbed at the interface. Figure 1(a) shows a series of dI/dV spectra taken along a line that crosses an hexagonal graphene island and contains one impurity [arrow in Fig. 1(a)]. The impurity consists of one or more Ni atoms that get trapped during the formation of the graphene islands [17]. Representative dI/dV spectra of the Ni surface, Ni impurity, and graphene nanoisland are shown in Fig. 1(b). The spectrum acquired on graphene shows two prominent peaks around E_F followed by a weaker and broad hump centered at about +0.80 eV. First principles calculations assign them to graphene π states [Fig. 1(c)], which split into spin-polarized gapped bands due to the strong hybridization with Ni d bands [13, 14, 19–21]. The spin-split Ni d-bands can be clearly identified as the two sharp peaks $d^{\uparrow}$ and $d^{\downarrow}$ in the impurity spectrum; on the Ni surface such peaks are masked by the dominant contribution of surface states, which we label as S_1 and S_2 following the nomenclature of previous studies [22–24] (further information on the electronic structure of the surface states can be found in Fig. S2 of the Supplementary Material).

In the following we will examine how the Ni surface states are affected by the interaction with graphene, and how this interaction is determinant for scattering at the graphene edge. The strong spatial variations of the dI/dV intensity outside the graphene island [green lines in Fig. 1(a)] are due to the quantum interference between incident and reflecting surface electrons. The interference patterns formed by S_1 at different energies are clearly visible in the dI/dV maps and profile shown in Fig. 2. This shows that the Ni surface states are very sensitive to the presence of graphene edges. Moreover, contrary to graphene nanoislands grown on Ir(111) [25, 26],

the wave patterns are absent inside the islands. Our *ab initio* calculations attribute this effect to the significant modification of the S_1 surface state below the graphene layer, which leads to a large energy mismatch of the surface state inside and outside the island. Such an energy mismatch depends strongly on the graphene-metal separation, as illustrated by the calculations reported in Fig. 3(a) for the majority electrons. As graphene is brought to the equilibrium distance of 2.1 Å with respect to the Ni surface plane, the S_1 state shifts in energy from slightly below E_F up to about 2.5 eV above E_F, and its spectral weight shifts towards the graphene-Ni interface [Fig. 3(b)]. This means that rather than being quenched, as concluded in Ref. 21, the surface state evolves into an interface state (IFS), as found for graphene-covered Ru(0001) [27]. The IFS can easily be identified in the constant current dI/dV spectra of Fig. 3(d). Here, field emission resonances (FER) that originate from the tip-induced Stark shift of image states are recognized by their upward energy shift when going from graphene to Ni, due to the higher work function of the latter [27, 28]. In contrast, the peak at 2.45 V is localized on the graphene island [Fig. 3(c)] and can thus be associated with the IFS predicted by our calculations at this energy. Such large energy shifts of the surface state only occur when graphene and metal states strongly hybridize and result in highly reflecting graphene edges. This is opposed to the case of less reactive metals such as Ir(111), where significant transmission of surface electrons across a graphene edge is possible due to the large energy overlap of states at the two sides [26].

The scattering of spin-split Ni surface states can lead to a lateral spin filtering effect similar to that mediated by bulk d states in the transport perpendicular to the graphene/Ni interface [13, 14]. We investigate this effect by analyzing the Fourier transform of the standing wave patterns shown in Fig. 2(b) [29]. We find a single dispersion curve [Fig. 4(a)] with no evidence for exchange-split bands. This curve is assigned to the majority $S_1^{\uparrow}$ sate, in agreement with all the band structure calculations reported to date, which predict $S_1^{\uparrow}$ to be partially occupied in clear contrast to the minority $S_1^{\downarrow}$ [19, 22, 23, 30, 31]. Another strong argument for such assignation is provided by the different surface character of majority and minority S_1 bands, as depicted in Fig. 4(b). The minority band, lying much closer to bulk states [19], presents a substantially shorter lifetime and a larger penetration into the bulk, illustrated in Fig. 4(b) by the density profile of each of those bands at Γ. At this point, $S_1^{\downarrow}$ overlaps with bulk bands and assumes a surface resonance character. Scattering to bulk states at the graphene edge further reduces the lifetime of $S_1^{\downarrow}$ electrons. This explains the dominant contribution of the majority states to the standing waves and supports the identification of the experimental curve in Fig. 4(a) with the dispersion of

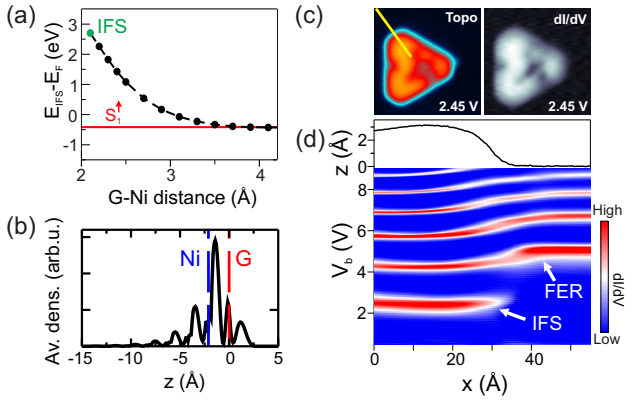

FIG. 3. (Color online) (a) Energy of the majority IFS as a function of the graphene-Ni distance. The energy of the S_1 state for pristine Ni(111) is represented by the red line. (b) Planar average of the density associated with the majority IFS at the equilibrium graphene-Ni distance (2.1Å). (c) Topographic and constant current dI/dV maps simultaneously acquired at the energy of the IFS. Setpoint current: $I = 1.2$ nA. Image size: 9.7×9.7 nm^2 (d) Topographic profile and constant current dI/dV spectra taken along a line that goes from Ni to a graphene island [yellow line in (c)], showing the IFS and the higher lying FERs. Setpoint values: $I = 1$ nA, $V_b = 0.1$ V.

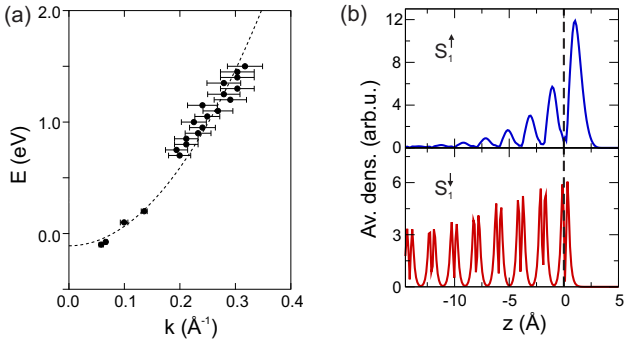

FIG. 4. (Color online) (a) Dispersion relation obtained from the standing wave periodicity. A parabolic curve is included for guiding (dashed line), with onset at -0.110 eV, as obtained from the dI/dV spectra. (b) Planar average density of the majority and minority S_1 states at the Γ point.

the $S_1^{\uparrow}$ band. The overall effect is a spin-dependent scattering that is mainly due to the different absorption to bulk states at the graphene edges, as opposed to the spin-dependent transmission in the scattering of Ni d states perpendicular to the interface [13, 14].

Finally, we investigate the influence of the edge geometry on electron scattering. Hexagonal islands are ideal for this purpose, since edges on adjacent sides present a distinct atomic structure, as shown in Fig. 5(a). The two different edge types correspond to an unreconstructed zig-zag edge (n) and a reconstructed edge (r) with double periodicity that is related to the so-called "57" reconstruction [32], in which the outermost hexagons are re-

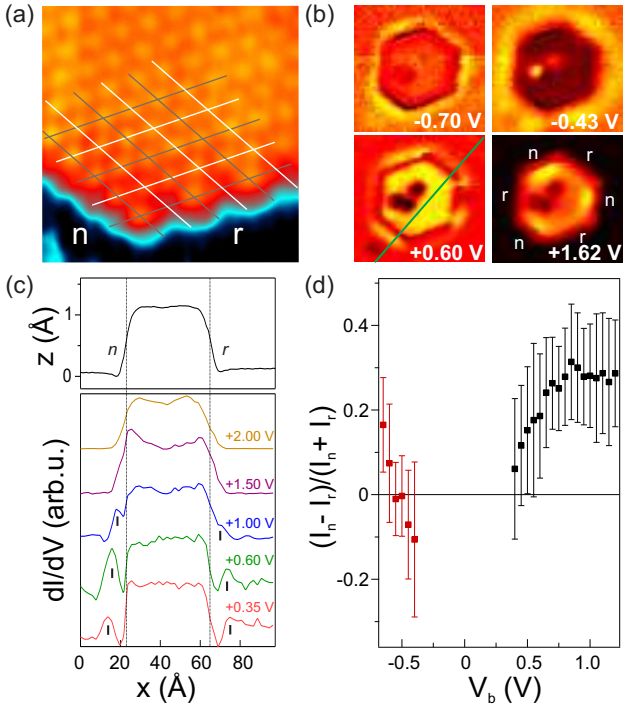

FIG. 5. (Color online) (a) Atomically resolved topographic image of the boundary of a graphene island, where reconstructed edges (r) exhibit twice the periodicity of the non-reconstructed ones (n). (b) Constant height dI/dV maps measured on a 50 × 50 grid on the hexagonal island of Fig. 1. Setpoint values: $I = 4$ nA, $V_b = -3.0$ V. (c) Topographic and dI/dV profiles taken along the green line in (b). For better visualization, the profiles are normalized by subtracting the dI/dV intensity of the Ni surface and divided by the intensity at the center of the island. (d) Asymmetry of the scattering intensity of n/r edges for the S_1 (black) and S_2 (red) surface state, as defined in the text. Error bars indicate the standard deviation of data obtained from different edges of the hexagon.

placed by pentagons and heptagons [2]. The asymmetry in the scattering amplitude at two opposite edges is evident in Figs. 5(b) and (c). From the spectroscopic images shown in (c) we observe that reconstructed edges produce weaker dI/dV oscillations at most energies. At +1.6 V, intensity modulations also appear at the graphene side of the edge, which could either indicate asymmetric scattering of the graphene bands in this energy range (see Fig. S3 in Ref. 19) or the presence of edge states. The asymmetry effect can be better quantified by measuring the dI/dV intensity ($I_{n,r}$) at the first maximum of the standing wave as a function of energy, indicated by ticks in Fig. 5(b). Both edges are excellent reflectors for the S_1 states due to the large energy shift of this band in the graphene covered region, which effectively inhibits transmission. Therefore, the peak intensity ratio for the two edge types is mainly determined by the differences in the reflection/absorption ratio [33]. Absorption here means both elastic and inelastic scattering into bulk states. Figure 5(d) shows the edge scattering asymmetry defined as the ratio $(I_n - I_r)/(I_n + I_r)$. Positive values ($I_n > I_r$) thus imply larger absorption at reconstructed edges . We see that, for S_1, the asymmetry increases as we go higher in energy (away from the Γ point), saturating at a value of about 30% at +0.8 V. The increment of the asymmetry is consistent with the periodicity doubling of the r-edge that, due to band folding, is likely to increase the absorption into bulk. On the other hand, the downwards dispersing S_2 band shows a more complex behavior, with a negative asymmetry at Γ that changes sign at lower energy. Therefore, the edge type, electron energy, and orbital composition of the surface state concur in determining the scattering asymmetry.

In conclusion, graphene nanoislands with well-defined edge geometry grown on Ni(111) allowed us to study the scattering of two-dimensional electrons parallel to the graphene/metal interface. The strong interaction between C and Ni atoms induces a significant energy mismatch of the surface bands inside and outside graphene, quenching the transmission through the graphene edge. In the case of the S_1 surface state of Ni, this effect is modulated by the different degree of coupling to bulk states of each spin-split band, leading to pronounced spin-dependent scattering that favors the reflection of majority electrons. The atomic edge structure has a significant influence on the scattering amplitude, leading to a scattering asymmetry for the majority S_1 band of up to 30%. These results elucidate the complex scattering properties of graphene/metal interfaces and are important for the control of electron transport and quantum confinement in lateral graphene junctions with spin-polarized electrodes.

We acknowledge support from the Basque Departamento de Educación, UPV/EHU (Grants No. IT-366-07 and IT-756-13), the Spanish Ministerio de Ciencia e Innovación (Grants No. FIS2010-19609-C02-00, MAT2007-62732, and MAT2010-15659), the ETORTEK program funded by the Basque Departamento de Industria, the European Research Council (StG 203239 NOMAD), and Agència de Gestió d'Ajuts Universitaris i de Recerca (2009 SGR 695). A.M. acknowledges funding from the Ramón y Cajal Fellowship program.

[1] A. H. C. Neto, F. Guinea, N. M. R. Peres, K. S. Novoselov, and A. K. Geim, Rev. Mod. Phys. **81**, 109 (2009).
[2] A. Rozhkov, G. Giavaras, Y. P. Bliokh, V. Freilikher, and F. Nori, Phys. Rep. **503**, 77 (2011).
[3] M. H. Rümmeli, C. G. Rocha, F. Ortmann, I. Ibrahim, H. Sevincli, F. Börrnert, J. Kunstmann, A. Bachmatiuk, M. Pötschke, M. Shiraishi, M. Meyyappan, B. Büchner, S. Roche, and G. Cuniberti, Adv. Mater. **23**, 4471 (2011).

[4] P. Y. Huang, C. S. Ruiz-Vargas, A. M. van der Zande, W. S. Whitney, M. P. Levendorf, J. W. Kevek, S. Garg, J. S. Alden, C. J. Hustedt, Y. Zhu, J. Park, P. L. McEuen, and D. A. Muller, Nature **469**, 389 (2011).

[5] A. W. Tsen, L. Brown, M. P. Levendorf, F. Ghahari, P. Y. Huang, R. W. Havener, C. S. Ruiz-Vargas, D. A. Muller, P. Kim, and J. Park, Science **336**, 1143 (2012).

[6] T. Shimizu, D. C. Haruyama, J. Marcano, D. V. Kosinkin, J. M. Tour, K. Hirose, and K. Suenaga, Nature Nanotech. **6**, 45 (2011).

[7] S. Roche, Nature Nanotech. **6**, 8 (2012).

[8] J. Fernández-Rossier and J. J. Palacios, Phys. Rev. Lett. **99**, 177204 (2007).

[9] G. Giovannetti, P. A. Khomyakov, G. Brocks, V. M. Karpan, J. van den Brink, and P. J. Kelly, Phys. Rev. Lett. **101**, 026803 (2008).

[10] P. Sutter, J. T. Sadowski, and E. Sutter, Phys. Rev. B **80**, 245411 (2009).

[11] P. Sutter, M. S. Hybertsen, J. T. Sadowski, and E. Sutter, Nano Lett. **9**, 2654 (2009).

[12] A. Varykhalov, J. Sánchez-Barriga, A. M. Shikin, C. Biswas, E. Vescovo, A. Rybkin, D. Marchenko, and O. Rader, Phys. Rev. Lett. **101**, 157601 (2008).

[13] V. M. Karpan, G. Giovannetti, P. A. Khomyakov, M. Talanana, A. A. Starikov, M. Zwierzycki, J. van den Brink, G. Brocks, and P. J. Kelly, Phys. Rev. Lett. **99**, 176602 (2007).

[14] J. Maassen, W. Ji, and H. Guo, Nano Lett. **11**, 151 (2011).

[15] M. Weser, Y. Rehder, K. Horn, M. Sicot, M. Fonin, A. B. Preobrajenski, E. N. Voloshina, E. Goering, and Y. S. Dedkov, Appl. Phys. Lett. **96**, 012504 (2010).

[16] O. M. J. van 't Erve, A. L. Friedman, E. Cobas, C. H. Li, J. T. Robinson, and B. T. Jonker, Nature Nanotech. **7**, 737 (2012).

[17] M. Olle, G. Ceballos, D. Serrate, and P. Gambardella, Nano Lett. **12**, 4431 (2012).

[18] J. M. Soler, E. Artacho, J. D. Gale, A. Garcia, J. Junquera, P. Ordejón, and D. Sanchez-Portal, J. Phys.: Condens. Matter **14**, 2745 (2002).

[19] See supplementary material at `http://link.aps.org/supplemental/xxx` for detailed explanation.

[20] M. Weser, E. N. Voloshina, K. Horn, and Y. S. Dedkov, Phys. Chem. Chem. Phys. **13**, 7534 (2011).

[21] L. V. Dzemiantsova, M. Karolak, F. Lofink, A. Kubetzka, B. Sachs, K. von Bergmann, S. Hankemeier, T. O. Wehling, , R. Frömter, H. P. Oepen, A. I. Lichtenstein, and R. Wiesendanger, Phys. Rev. B **84**, 205431 (2011).

[22] J. Lobo-Checa, T. Okuda, M. Hengsberger, L. Patthey, T. Greber, P. Blaha, and J. Osterwalder, Phys. Rev. B **77**, 075415 (2008).

[23] T. Ohwaki, D. Wortmann, H. Ishida, S. Blügel, and K. Terakura, Phys. Rev. B **73**, 235424 (2006).

[24] Y. Nishimura, M. Kakeya, M. Higashiguchi, A. Kimura, M. Taniguchi, H. Narita, Y. Cui, M. Nakatake, K. Shimada, and H. Namatame, Phys. Rev. B **79**, 245402 (2009).

[25] S. J. Altenburg, J. Kröger, T. O. Wehling, B. Sachs, A. I. Lichtenstein, and R. Berndt, Phys. Rev. Lett. **108**, 206805 (2012).

[26] D. Subramaniam, F. Libisch, Y. Li, C. Pauly, V. Geringer, R. Reiter, T. Mashoff, M. Liebmann, J. Burgdörfer, C. Busse, T. Michely, R. Mazzarello, M. Pratzer, and M. Morgensten, Phys. Rev. Lett. **108**, 046801 (2012).

[27] B. Borca, S. Barja, M. Garnica, D. Sánchez-Portal, V. M. Silkin, E. V. Chulkov, C. F. Hermanns, J. J. Hinarejos, A. L. Vázquez de Parga, A. Arnau, P. M. Echenique, and R. Miranda, Phys. Rev. Lett. **105**, 036804 (2010).

[28] P. A. Khomyakov, G. Giovannetti, P. C. Rusu, G. Brocks, J. van den Brink, and P. J. Kelly, Phys. Rev. B **79**, 195425 (2009).

[29] L. Simon, C. Bena, F. Vonau, M. Cranney, and D. Aubel, J. Phys. D: Appl. Phys. **44**, 464010 (2011).

[30] J. Braun and M. Donath, Europhys. Lett. **59**, 592 (2002).

[31] G. Bertoni, L. Camels, A. Altibelli and V. Serin, Phys. Rev. B **71**, 075402 (2004).

[32] M. Olle, A. Garcia-Lekue, D. Sanchez-Portal, A. Mugarza, G. Ceballos, and P. Gambardella, unpublished.

[33] The position of the first maximum with respect to graphene edges, measured at +0.35 V and +0.60 V, only differs by 7-15% between the two type of edges, indicating minor variations in the phase shift, and hence confirming the negligible role of transmission.